



# Influence of annealing on the structure and wear resistance of coatings produced by cold spraying of Al-SHS7574 powder mixture

Ivanna D. Kuchumova<sup>a,b,\*</sup>, Vladislav S. Shikalov<sup>c</sup>, Tomila M. Vidyuk<sup>c</sup>, Arina V. Ukhina<sup>d</sup>, Tatyana A. Brusentseva<sup>c</sup>, Ivan A. Bataev<sup>b</sup>

<sup>a</sup> Lavrentyev Institute of Hydrodynamics SB RAS, 15, Lavrentyev Ave., Novosibirsk 630090, Russia

<sup>b</sup> Novosibirsk State Technical University, 20, K. Marx Ave., Novosibirsk 630073, Russia

<sup>c</sup> Khristianovich Institute of Theoretical and Applied Mechanics SB RAS, 4/1, Institutskaya St., Novosibirsk 630090, Russia

<sup>d</sup> Institute of Solid State Chemistry and Mechanochemistry SB RAS, 18, Kutateladze St., Novosibirsk 630128, Russia



## ARTICLE INFO

### Keywords:

Aluminum  
Powder mixtures  
Partially amorphous  
Cold spraying  
Reaction layer  
Wear resistance

## ABSTRACT

In present work, the possibility of fabricating a composite cold-sprayed coatings consisting of partially amorphous alloy reinforcing particles and an aluminum matrix was studied for the first time. A mixture of pure aluminum and SHS7574 powders in a ratio of 50/50 wt% was deposited on aluminum alloy substrates, which ensured the formation of high-quality coating with a porosity of less than 1%. The ratio of SHS7574 alloy to aluminum in the as-sprayed samples was nearly the same as in the initial powder mixture which indicates a similar efficiency of component deposition. Composite coatings were annealed in a vacuum furnace at 540 °C and 600 °C. Microstructure and phase composition of as-sprayed and annealed coatings were examined with XRD, SEM and EDX mapping. Post annealing of the coatings promoted the formation of a reaction layers around the Fe-based alloy particles consisting of Fe<sub>2</sub>Al<sub>5</sub>, Fe<sub>4</sub>Al<sub>13</sub>, Fe<sub>23</sub>B<sub>5</sub>, and Fe<sub>5</sub>C<sub>2</sub> phases. The effect of annealing on the mechanical properties of the Al-SHS7574 coatings was determined by measuring hardness, nanohardness and wear resistance according to ASTM G 133-05. The increase in the samples' hardness after annealing was associated with the formation of a reaction layers and increase in its thickness with rising annealing temperature. The coating annealed at 600 °C demonstrated the highest hardness due to the formation of thick brittle reaction layers. The preservation of the aluminum matrix with the simultaneous formation of thin reaction layers after annealing at 540 °C reduced the wear rate of the coating despite the moderate hardness.

## 1. Introduction

Cold sprayed aluminum-based coatings are used as protective layers for various applications. For example, aluminum coatings are applied to improve heat transfer in the nuclear power industry and to protect against corrosion in an aqueous environment [1–3].

Cold spraying can also be used to form coatings with an amorphous structure [4]. The temperature of the gas flow during the cold spraying process does not exceed melting point of the aluminum powder [5]. Therefore, the probability of particles oxidation, decarburization, formation of high residual stresses, decomposition, sublimation and other negative processes typical for high-temperature thermal spraying methods, such as plasma spraying, detonation spraying and high-velocity oxy-fuel spraying (HVOF), are reduced. Powders with original amorphous structure and particle size of 10–40 µm could be

used to obtain coatings by cold spray method. During the spraying process, the powders are heated to the temperature of a supercooled liquid (between the glass transition and crystallization temperatures) and are deformed upon impact with the substrate. Tului et al. studied the structure and properties of coatings obtained from commercial powder alloy SHS7574 (Nanosteel Company Inc., Providence, RI, USA) by HVOF and cold spraying [6]. They showed that cold spraying allowed the formation of coatings with a denser structure and a higher amorphization degree compared to the HVOF method. Although the initial powder had a nanocrystalline structure, the deformation during the cold spraying was so large that it destroyed the crystalline structure, thus allowing formation of amorphous coatings.

The formation of multifunctional coatings combining several functional properties is one of the main trends in modern spraying technologies. Composite multifunctional coatings can be fabricated in three

\* Corresponding author at: Lavrentyev Institute of Hydrodynamics SB RAS, 15, Lavrentyev Ave., Novosibirsk 630090, Russia.  
E-mail address: [ivannakz@mail.ru](mailto:ivannakz@mail.ru) (I.D. Kuchumova).

**Table 1**  
Parameters of dry linearly reciprocating sliding conditions.

Parameters	Values
Sliding frequency, Hz	5
Stroke length, mm	5
Applied load, N	25
Total sliding distance, m	100

different ways: spraying of powder mixtures [7,8], spraying of composite powders obtained by mechanical milling [9,10], and spraying of coated powders [11]. Cold spraying of powder mixtures and its additional heat treatment is one of the main methods for obtaining multifunctional coatings [12]. The possibility of intermetallic phases formation during heat treatment makes Fe-Al [13], Ti-Al [14], Zn-Al [15] coatings promising for fabrication the protective layers with high hardness, wear resistance, and fracture toughness. Wang et al. studied Fe-Al cold-sprayed coatings annealed at temperatures of 500, 600, 700, and 900 °C [16]. After annealing at 600 °C the Al<sub>5</sub>Fe<sub>2</sub> phase was formed and distributed between iron and aluminum particles. Annealing at 900 °C produced FeAl intermetallic phases with a small amount of remaining  $\alpha$ -Fe phase. However, the effect of the intermetallic phases on coating properties was not discussed.

The use of powders of glassy alloys as reinforcing particles in bulk composites is a promising trend [17]. Hot pressing and spark plasma sintering (SPS) are used for fabrication of bulk materials with aluminum matrix and reinforcing amorphous particles. While hot pressing often leads to complete or partial crystallization of the amorphous particles, SPS allows the amorphous structure to be preserved by reducing the duration of the synthesis. Dudina et al. discussed the effect of the SPS temperature on the structure and properties of Al-Fe<sub>66</sub>Cr<sub>10</sub>Nb<sub>5</sub>B<sub>19</sub> composites [18]. At a temperature of 540 °C they observed formation of a reaction layers consisting of different iron aluminides around the particles of amorphous alloy. Increasing the synthesis temperature to 570 °C increased the thickness of the reaction layer. Herewith, it should be noted that the amorphous alloy particles retained the metastable structure due to sintering in the supercooled liquid region. The formation of the reaction layer increased the hardness of the composites.

Aluminum metal matrix coatings are a class of materials which meets most of the rigorous specifications in applications where superior resistance to corrosion and good thermal and electrical conductivities are required [19]. Fe-based SHS7574 alloy has high corrosion and wear resistance. Reinforcing of aluminum matrix by amorphous alloy powder is a relatively new research concept. In present work, we attempt to obtain relatively lightweight and wear-resistant composite coatings for production and recovery of cylinder sleeves in engines, piston-recess

walls, brake discs or pads [20,21]. Several studies (see, for instance, [22,23]) showed that the reaction layers formed after heat treatment of Al-based nanocomposite reinforced with metallic glass nanoparticles increased the strength, hardness and wear resistance of the composite material and did not reduce its corrosion resistance.

The goal of the present work was to study the effect of the annealing

**Table 2**

Results of EDS analysis of aluminum and SHS7574 powders in powder mixture (rectangles in (Fig. 1b) are the areas selected for EDS analysis).

Chemical element, wt%	Aluminum powder	SHS7574 powder
	Spectrum 1	Spectrum 2
O	2.15	—
C	—	5.01
Si	—	1.50
Cr	—	18.64
Mn	—	2.27
Fe	—	51.16
Mo	—	14.93
W	—	6.50
Al	97.85	—
Totals	100	100

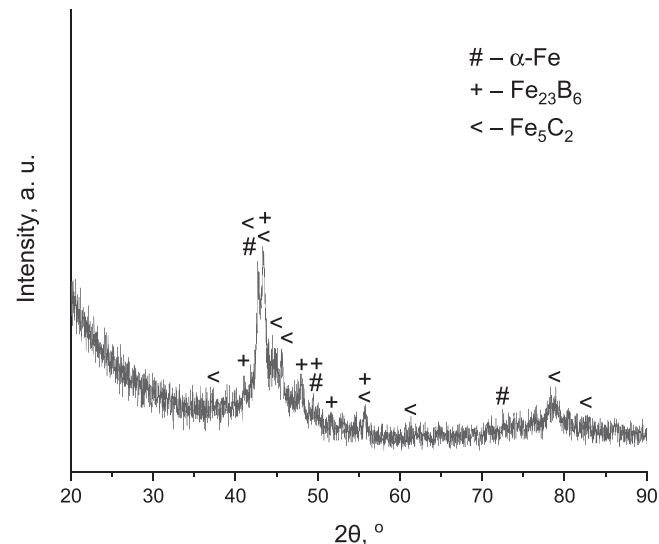
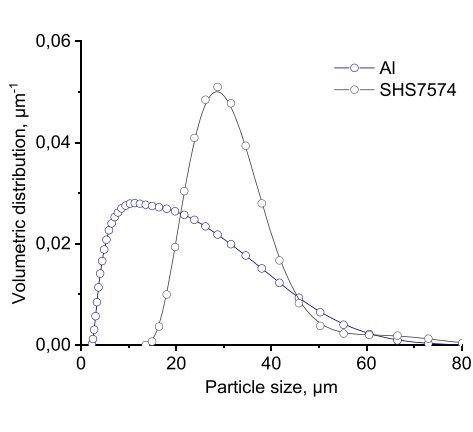
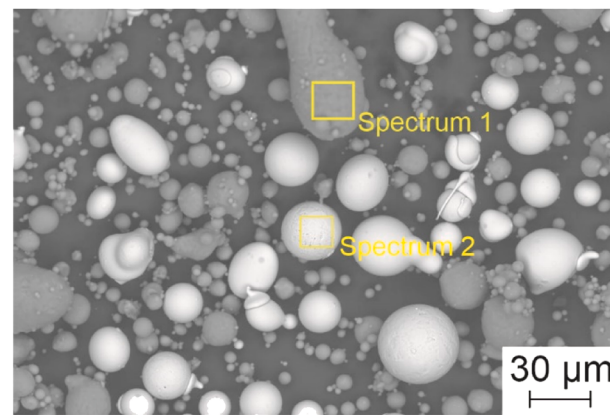


Fig. 2. XRD pattern of SHS7574 powder.



a



b

Fig. 1. The particle size distribution of the Al and SHS7574 starting powders (a) and SEM image of the Al-SHS7574 powder mixture (b). Micrograph was obtained by SEM in the BSE emission mode.

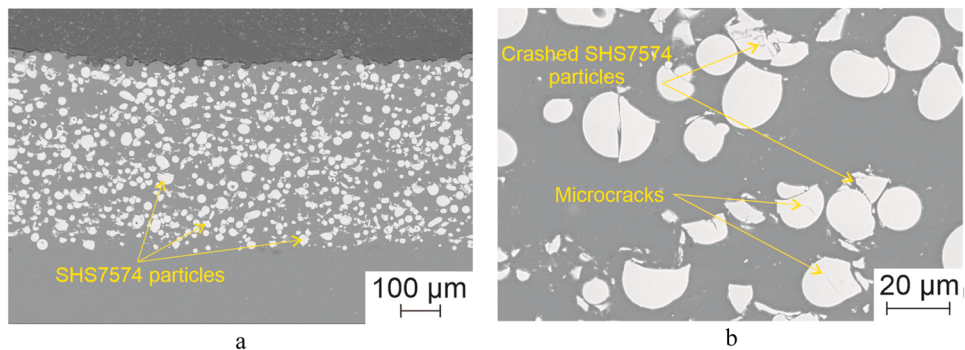


**Fig. 3.** Cross-section images of the as-sprayed Al-SHS7574 coating: (a) overview and (b) high-magnification. Micrographs were obtained by SEM in the BSE emission mode.

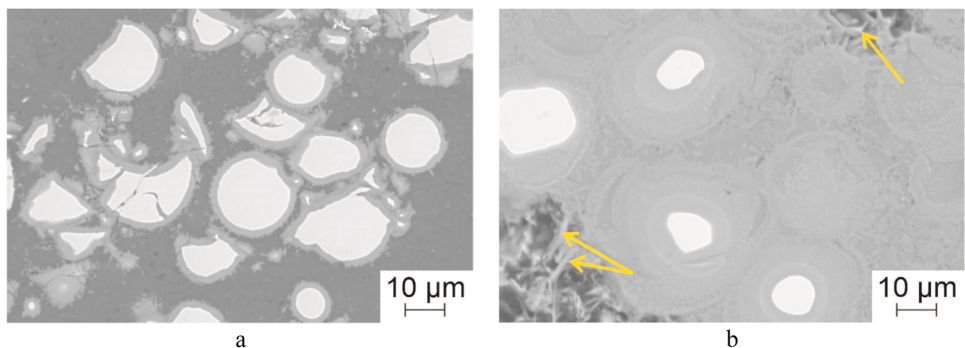


**Fig. 4.** Cross-section images of the cold-sprayed Al-SHS7574 coatings after annealing at different temperatures: (a) 540 °C; (b) 600 °C. The arrows in (b) indicate the plate-shaped structures (b). Micrographs were obtained by SEM in the BSE emission mode.

on the phase composition, microstructure, hardness and wear resistance of the cold sprayed aluminum coatings reinforced with Fe-based partially amorphous alloy powder. The influence of heat treatment on the phase composition and microstructure of the composite coatings was investigated by X-ray diffraction (XRD) and scanning electron microscopy (SEM). The influence of the reaction layer on the properties of the composite coatings was investigated by Vickers hardness measurements and ball-on-flat sliding wear tests.

## 2. Materials and methods

Aluminum (15–40 μm, 99.2 wt% pure aluminum, ASD-1, Russia) and Fe-based alloy SHS7574 (15–40 μm, The LincolnElectric Company, USA) powders were used for cold spraying. The chemical composition of SHS7574 powder was: B = 2.96; Cr = 17.78; Mn = 2.10; Mo = 14.24; W = 5.90; C = 0.88; Al < 0.05; Co = 0.06; Cu = 0.09; Nb < 0.02; Ni = 0.13; P = 0.016; Si = 1.36; Sn < 0.02; Ta < 0.02; Ti < 0.02; V = 0.05; Fe – balance (all in wt%). The Al-SHS7574 powder mixture in a ratio of 50/50 vol% was prepared using a V-shaped mixer (Filtral Vibracion, Spain). This ratio of components was chosen to compare the properties, phase composition and microstructure of the coatings with the results of Dudina et al. [18], Balci et al. [24] and Wang et al. [25], who used the addition of 40–60 vol% amorphous alloy powder to the aluminum matrix for production of bulk composites.”

Aluminum alloy plate (Grade AMG2M, GOST 21631–76, analog to ISO 209–1 AlMg2) with the dimensions of 50 × 50 × 4 mm<sup>3</sup> was used as substrates. Before the spraying, the substrate was grit-blasted with alumina abrasive. The coating was sprayed on an experimental high-pressure cold spraying facility (ITAM SB RAS, Russia), described in detail in [26], using an axisymmetric de Laval nozzle OUT1 (Impact Innovations GmbH, Germany). Air at a stagnation pressure of 4 MPa and a stagnation temperature of 300 °C was used as an accelerating gas. The

standoff distance was 30 mm. The nozzle was moved relative to the substrate at a speed of 200 mm s<sup>-1</sup> with an offset step of 3 mm to obtain a continuous coating layer on the entire surface of the substrate. For the second layer, the substrate was rotated by 90°.

The coatings were annealed in the vacuum furnace (VSE\_VACUUM FURNACE, Russia) at temperatures of 540 °C and 600 °C and a pressure of 1.33•10<sup>-3</sup> Pa (9.98•10<sup>-6</sup> mmHg). The samples were heated to the selected temperature at a rate of 10 °C s<sup>-1</sup>. After holding for two hours, the samples were cooled down with the furnace.

XRD analysis of the feedstock powders, initial powder mixture, as-sprayed coatings and annealed coatings were carried out using a Bruker D8 ADVANCE diffractometer (Bruker AXS, Germany). The morphology of the Al-SHS7574 powder mixture and the microstructure of the samples (as-sprayed and annealed) were studied using scanning electron microscope (SEM) EVO MA15 (Zeiss, Germany) coupled with energy-dispersive X-ray spectrometer (EDS) X-Max 80 mm<sup>2</sup> (Oxford Instruments, UK). The porosity, thickness of as-sprayed coatings, thickness of reaction layers in heat-treated coatings and the content of SHS7574 particles in the composite coatings were determined using the OLYMPUS Stream Image Analysis Software "Stream Essentials 1.9.1" (OLYMPUS, Japan) from ten cross-sectional SEM micrographs.

Cross-sectional specimens for microstructural, nanohardness and microhardness studies, as well as surface samples for wear resistance tests were grinded and polished to roughness R<sub>a</sub> = 0.04 μm. XRD analysis was performed on the as-sprayed and as-annealed surface of the Al-SHS7574 coatings.

The hardness of the coating was measured on cross-sections of the as-sprayed and annealed coatings using a Vickers hardness testing device (402MVD, Wolpert Wilson Instruments, Germany) under 1 kg load with holding time of 15 s. The microhardness of SHS7574 alloy particles in as-sprayed and annealed coatings was measured at a load of 0.05 kg. More than 10 hardness values were obtained to calculate the average.

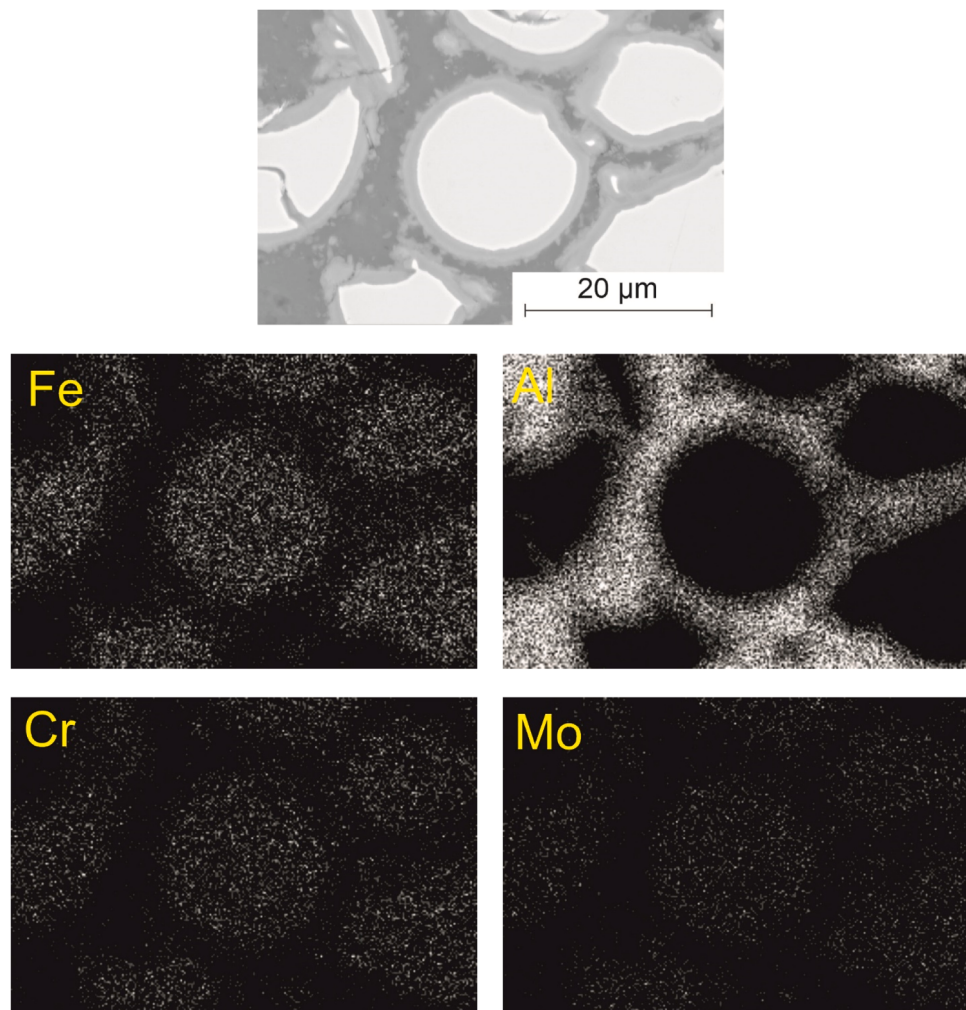


**Fig. 5.** SEM image and elemental distribution maps of Fe, Al, Cr, and Mo, which were obtained from the selected cross-section areas of the Al-SHS7574 coatings after annealing at 540 °C during 2 h. Micrograph was obtained by SEM in the BSE emission mode.

The nanohardness of the coatings after the heat treatment was measured on a polished surface using a scanning nanohardness tester Nanoscan 4D+ (TISNCM, Russia) with a standard Berkovich tip according to the standardized Oliver and Pharr method [27]. The areas with reaction layer were selected for the measurements. For nano-indentation tests, a normal load of 15  $\mu$ N, an indentation rate of 100 nm s $^{-1}$  and a peak load holding time of 2 s were used. The average nanohardness values and the confidence intervals were calculated based on 10 measurements.

The dry sliding wear test of as-sprayed and annealed cold sprayed coatings was performed using an UMT-2 tribometer (Bruker, Germany) operating in the linearly reciprocating sliding mode. The dry sliding friction test scheme was chosen due to the expected practical application of the composite coatings. The WC-6Co ball with diameter of 6.35 mm was used as a counterpart. Before the wear tests, the coatings were grinded and polished. The roughness of the samples after polishing using colloidal silica suspension was  $R_a \approx 0.04$   $\mu$ m. The WC-6Co balls' roughness (as-received condition) was  $R_a \approx 0.1$   $\mu$ m. Table 1 shows the parameters of dry linearly reciprocating sliding conditions. After the wear tests, the volume loss was determined by optical profilometry (Contour GT-K1 3D, Bruker) and analyzed with Vision64 software. Average values of volume loss were calculated after 5 measurements. The confidence intervals are given for a confidence level of 0.95. The worn surfaces were studied using SEM.

### 3. Results and discussion

#### 3.1. Characterization of the feedstock powders and initial Al-SHS7574 powder mixture

Fig. 1 shows the distribution of particle size of aluminum and SHS7574 powders and morphology of the Al-SHS7574 powder mixture. The average particle size was 27  $\mu$ m and 35  $\mu$ m for the aluminum and SHS7574 powders, respectively (Fig. 1a). The particles of both powders had spherical or close to spherical shape (Fig. 1b). The results of the elemental analysis of the surfaces of Al-SHS7574 powder mixture are shown in Table 2 (from rectangles in Fig. 1b). The EDS analysis confirmed the content of main elements in SHS7574 alloy powder (Si, Cr, Mn, Fe, Mo, W). The carbon content differed from original chemical composition, and boron was not detected due to the low sensitivity of EDS method to light elements (nitrogen, oxygen, boron and oxygen). Elements (such as Al, Ta, Ti, V) with content below 0.1 wt% also were not observed. Insignificant amount of oxygen was detected on the surface of the aluminum particles. The XRD pattern of the SHS7574 powder (Fig. 2) demonstrated a broad halo between  $2\theta = 35\text{--}50^\circ$ , indicating the presence of an amorphous phase. The feedstock SHS7574 powder was characterized by the presence of  $\alpha$ -Fe, Fe<sub>23</sub>B<sub>6</sub>, and Fe<sub>5</sub>C<sub>2</sub> crystalline phases.

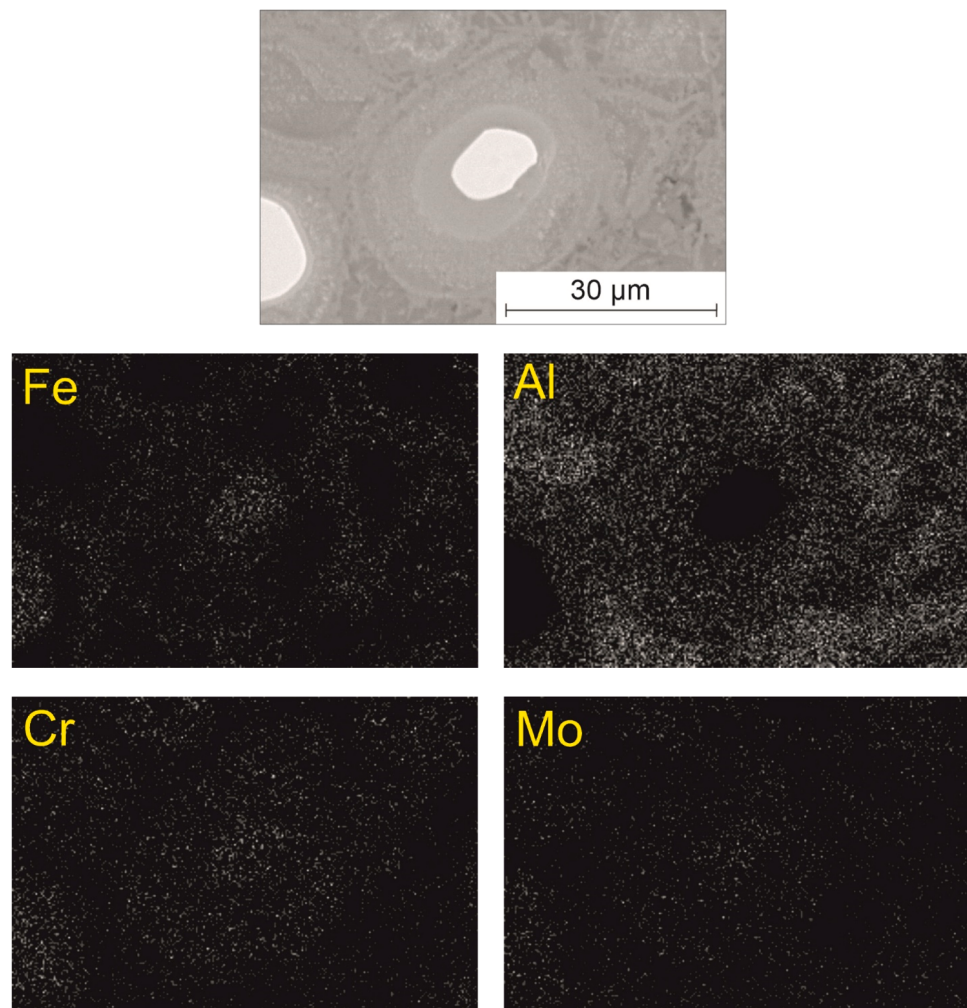


**Fig. 6.** SEM image and elemental distribution maps of Fe, Al, Cr, and Mo, which were obtained from the selected cross-section areas of the Al-SHS7574 coatings after annealing at 600 °C during 2 h. Micrograph was obtained by SEM in the BSE emission mode.

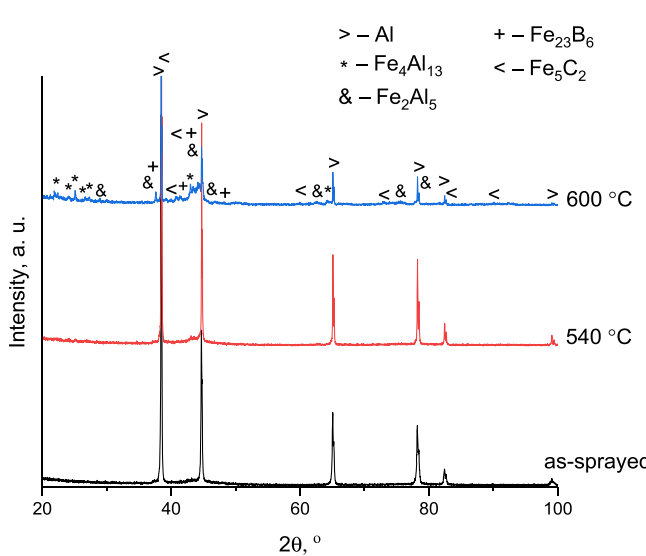


**Fig. 7.** The XRD patterns of the as-sprayed and annealed Al-SHS7574 coatings.

### 3.2. Microstructure and phase composition of coatings

The cross-sections of the as-sprayed coating are shown in Fig. 3. The average content of Fe-based powder (indicated by arrows in Fig. 3a) was approximately 48 vol%, which is very close to its content in the feedstock mixture (50/50 vol%). This fact indicates a close deposition efficiency of both powders at selected spraying modes. It should be noted that such behavior is not entirely typical for cold spraying of powder mixtures, since the coating composition usually differs significantly from that of the starting mixture [8,28]. Fe-based alloy particles kept spherical shape and were relatively uniformly distributed in the aluminum matrix. Due to the low ductility of partially amorphous alloy, microcracks and some crushed particles are visible in the volume of some Fe-based alloy particles (indicated by arrows in Fig. 3b). Being softer than SHS7574 particles, aluminum deformed more easily and created a uniform pore-free matrix, in which Fe appeared as isolated particles. As-sprayed coatings show dense structure with a porosity of less than 1%. The thickness of as-sprayed coatings was  $485 \pm 15 \mu\text{m}$ . The results of bonding strength determination of aluminum coatings produced by cold spraying on stainless steel substrates has been reported in our previous studies [29,30]. The adhesive strength of pure ASD-1 coatings was 15–20 MPa.

Fig. 4 shows enlarged micrographs of Al-SHS7574 coatings after annealing at 540 °C and 600 °C. Annealing at 540 °C resulted in the growth of the reaction layer with a thickness of  $2.55 \pm 0.10 \mu\text{m}$  (light-gray phase in Fig. 4a) around Fe-based alloy particles (almost white in

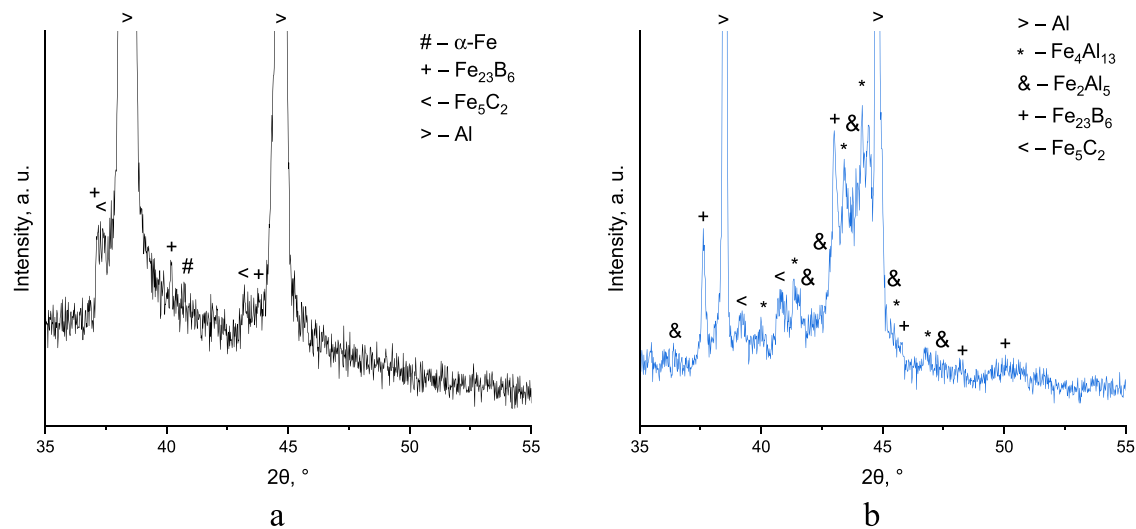


**Fig. 8.** Enlarged areas of the XRD patterns ( $2\theta = 35\text{--}50^\circ$ ) of the coatings after cold spraying (a) and after heat treatment at  $600\text{ }^\circ\text{C}$  (b).

**Table 3**

Porosity and Vickers hardness of the cold-sprayed and annealed Al-SHS7574 coatings and microhardness of SHS7574 particles. The confidence intervals are given for a confidence level of 0.95.

Coating material and annealing temperature	Porosity, %	Hardness of the coatings, GPa	Microhardness of SHS7574 particles, GPa
Al-SHS7574, 0 °C	< 1	$0.60 \pm 0.05$	$10.45 \pm 0.03$
Al-SHS7574, 540 °C	< 1	$0.78 \pm 0.05$	$11.90 \pm 0.15$
Al-SHS7574, 600 °C	$25 \pm 5$	$3.53 \pm 0.25$	-

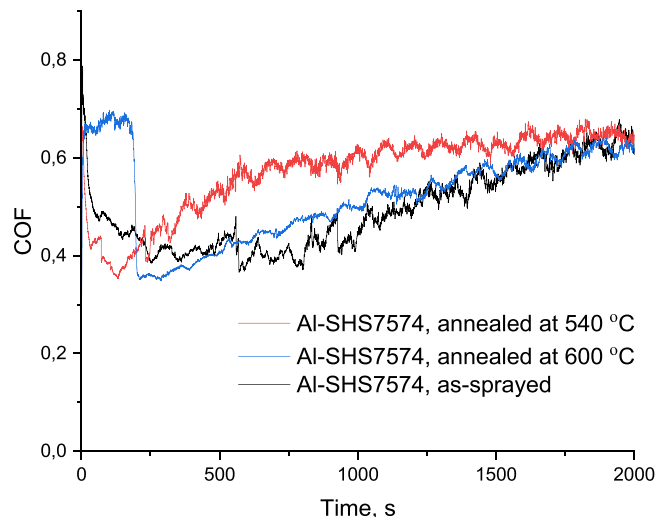


**Fig. 9.** Coefficient of friction (COF) of the Al-SHS7574 coatings plotted versus test time.

**Table 4**

Volume loss and COF of the composite coatings. The confidence intervals for volume loss are given for a confidence level of 0.95.

Coating material and annealing temperature	Volume loss, mm <sup>3</sup>	Average COF in steady-state stage
Al-SHS7574, 0 °C	$0.65 \pm 0.06$	0.47
Al-SHS7574, 540 °C	$0.50 \pm 0.02$	0.57
Al-SHS7574, 600 °C	$1.05 \pm 0.21$	0.52

**Fig. 4a)**. The porosity of the coatings after annealing at  $540\text{ }^\circ\text{C}$  was less than 1%. Increasing the annealing temperature promoted the growth of the reaction layer (**Fig. 4b**). After the heat treatment at  $600\text{ }^\circ\text{C}$ , aluminum was fully consumed so that the reaction layers around the particles touched each other and could not grow further. Plate-shaped structures indicated with arrows in **Fig. 4b** were observed in the sample. The formation of such structures was associated with local aluminum melting during the exothermal reaction between aluminum and SHS7574 powder. Annealing of the coatings at  $600\text{ }^\circ\text{C}$  led to an increase in porosity (up to  $25 \pm 5\%$ ), which is associated with the Kirkendall effect [31]. During the heat treatment of the coatings obtained from two heterogeneous powders, which have significantly different melting points, the atoms of the more active material (in this case, aluminum) diffused faster. As a result, the interface between the two materials shifted and the formation of pores and plate-shaped structures occurred. Determining the phase composition of these structures is a challenging task.

The formation of the similar plate-shaped crystals during sintering was previously discussed by Dudina et al. [32]. The Al-70 vol% Fe<sub>66</sub>Cr<sub>10</sub>Nb<sub>5</sub>B<sub>19</sub> obtained by SPS had pores with nearly spherical shape which were surrounded by plate- and needle-shape crystals. The phase composition of these crystals was corresponded to the mixture of Fe<sub>4</sub>Al<sub>13</sub> and Fe<sub>2</sub>Al<sub>5</sub>.

Fe, Al, Cr, and Mo elemental maps of the annealed samples are shown in **Fig. 5** ( $540\text{ }^\circ\text{C}$ ) and **Fig. 6** ( $600\text{ }^\circ\text{C}$ ). It should be noted that, as boron and carbon are a low-Z elements, it was quite difficult to obtain reliable information on their concentration. Thus, the structure and spatial distribution of boron- and carbon-containing phases in annealed coatings remain an open question requiring further investigation. In the coatings annealed at  $540\text{ }^\circ\text{C}$ , most of the iron was concentrated in the Fe-based alloy particles and the aluminum was in the matrix (**Fig. 5**). The elemental maps confirmed the presence of both iron and aluminum in the reaction layers around the SHS7574 particles. The increase in the thickness of the reaction layer around the Fe-based alloy particles (after heat treatment at  $600\text{ }^\circ\text{C}$ ) leads to a relatively uniform distribution of iron and aluminum in the coating structure (**Fig. 6**). After annealing at  $540\text{ }^\circ\text{C}$  Mo and Cr are predominantly contained in the Fe-based alloy particles. Annealing at  $600\text{ }^\circ\text{C}$  favored the diffusion of Mo and Cr into the reaction layers, therefore providing formation of intermetallics, borides and carbides of these elements.

**Fig. 7** shows the XRD patterns of the as-sprayed and annealed coatings. No aluminum or iron oxides were observed in the as-sprayed sample due to the low temperature of the cold spray process. The XRD pattern of the cold-sprayed coating has no reflection of the reaction

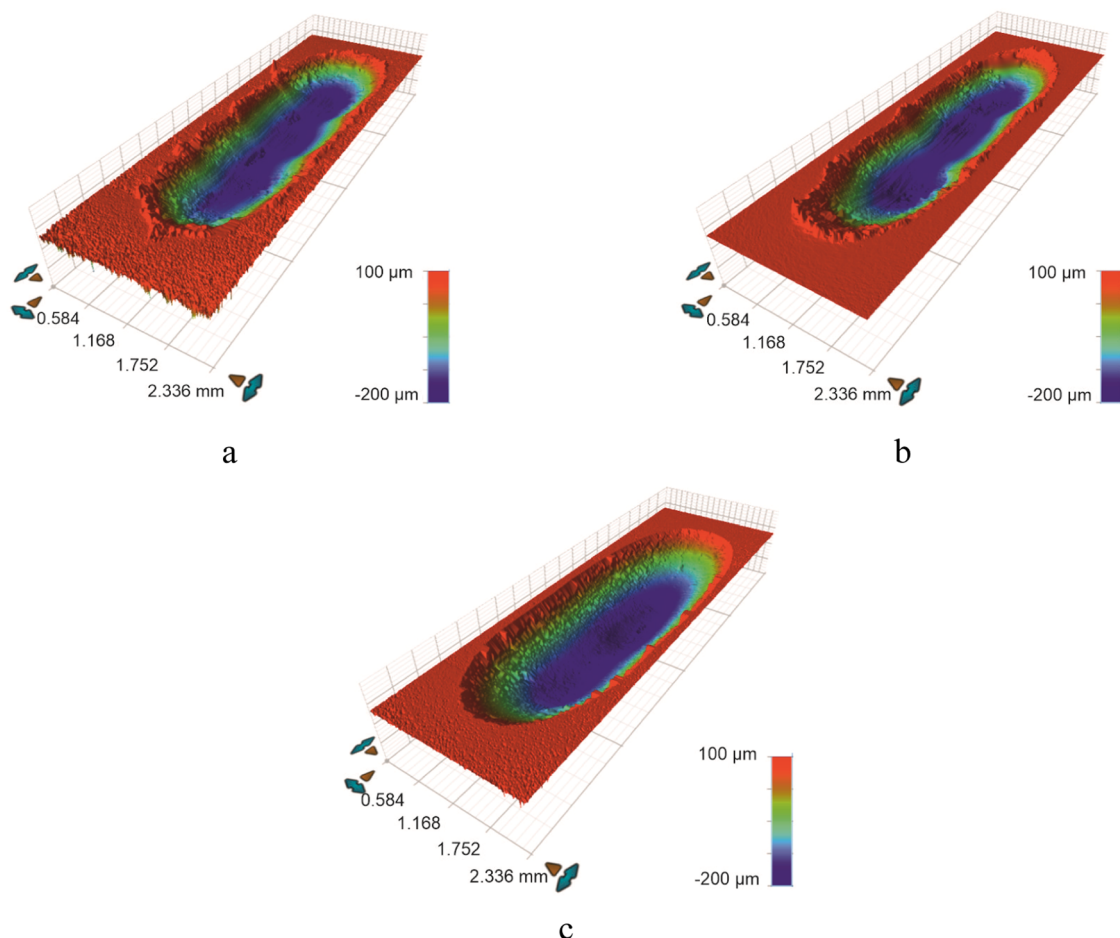


**Fig. 10.** . 3D optical profilometer images of wear tracks of Al-SHS7574 coatings: a – as-sprayed; b – annealed at 540 °C; c – annealed at 600 °C.

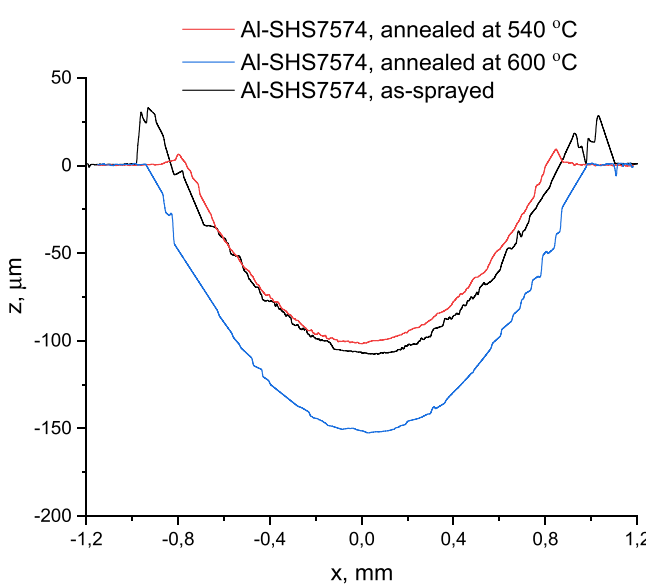


**Fig. 11.** The cross-sectional 2D profiles of worn surfaces of the Al-SHS7574 coatings.

products of aluminum and Fe-based alloy. After annealing at 540 °C, the coating contained  $\text{Fe}_4\text{Al}_{13}$  ( $\text{FeAl}_3$ ) and  $\text{Fe}_2\text{Al}_5$  phases in reaction layers. In the literature the formula  $\text{FeAl}_3$  is mainly used to describe the Al-rich phase in the Fe-Al system. With increasing the annealing temperature

the content of  $\text{Fe}_4\text{Al}_{13}$  and  $\text{Fe}_2\text{Al}_5$  phase increased due to formation of broad reaction layers. Enlarged areas of the XRD patterns ( $2\theta = 35\text{--}50^\circ$ ) of the coatings after the cold spraying and annealing at 600 °C are shown in Fig. 8. It can be seen that the intensity of the  $\text{Fe}_{23}\text{B}_5$  and  $\text{Fe}_5\text{C}_2$  reflections increased, which is associated with complete crystallization of the SHS7574 alloy. Although the microstructure images of the coatings after annealing at 600 °C showed almost no areas of the Al matrix (Fig. 4b); it can be concluded from the XRD pattern that aluminum is still contained in the coating.

### 3.3. Hardness and wear resistance of the coatings

The hardness of the as-sprayed and annealed at 540 °C and 600 °C coatings was 0.60 GPa, 0.78 GPa and 3.53 GPa, respectively (Table 3). Growth in the hardness of the coatings after annealing was associated with the formation of the reaction layers and increasing its thickness. In addition, the microhardness of the SHS7574 alloy particles was measured. Annealing of the coatings at 540 °C contributed to increasing the SHS7574 hardness from 10.45 GPa up to 11.90 GPa due to crystallization of the partially amorphous alloy [33]. The microhardness of the SHS7574 particles after annealing at 600 °C was not measured because of its small size. The nanohardness of the reaction layers after annealing at 540 °C and 600 °C was  $15.5 \pm 0.9$  GPa and  $15 \pm 0.7$  GPa, respectively. Due to the formation of hard intermetallics, borides and carbides, the hardness of the reaction layers is significantly higher than that of the SHS7574 alloy particles. Cho et al. [34] showed that, the nanohardness of  $\text{FeAl}_3$  and  $\text{Fe}_2\text{Al}_5$  phases in press-hardened steel with Al–Si coatings was 5.2 GPa and 13.0 GPa, respectively. It can be assumed that the high nanohardness values of the reaction layers in Al-SHS7574 coatings after

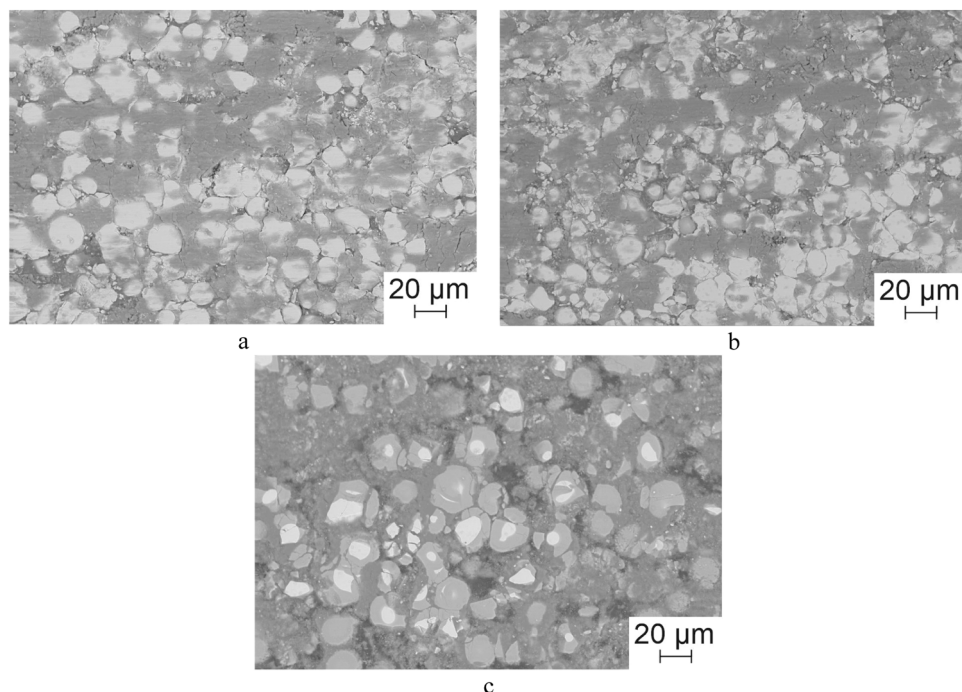


**Fig. 12.** The worn surface of the composite Al-SHS7574 coatings: a – as-sprayed; b – after annealing at 540 °C; c – after annealing at 600 °C. Micrographs were obtained by SEM in the BSE emission mode.

annealing are most likely associated with complex structure, which consists of high hardness components (carbides and borides).

Fig. 9 presents the coefficient of friction (COF) plotted versus the testing time measured under dry linearly reciprocating sliding conditions. It can be seen that the coatings reach steady-state stage after 500–600 s. The annealed at 540 °C coating had higher and more stable COF, which is indirect evidence of the higher wear resistance of the coating. More stable COF behavior indicates an even coating wear process. The COF leaps in the steady-state stage are attributed to the features of the ball-on-flat linearly reciprocating sliding condition. The delaminated particles during the test could not be removed from the friction surface, acting as abrasive particles and increasing the intensity of wear [35,36]. The higher COF (up to 200 s) of the sample annealed at 600 °C is probably due to delamination of the top layer of the coating.

The volume loss and average COF in steady-state stage of the composite coatings are summarized in Table 4. The volume loss of the as-sprayed and annealed at 540 °C and 600 °C coatings was 0.65 mm<sup>3</sup>, 0.50 mm<sup>3</sup> and 1.07 mm<sup>3</sup>, respectively. The formation of thin reaction layers (thickness 10–20 µm) composed of intermetallics, borides and carbides improved the wear resistance of the composite coatings after heat treatment at 540 °C. Annealing at 600 °C reduced the wear resistance of the coating material due to the significant increase in the thickness of the reaction layers. Dudina et al. [37] reported, that increasing of the sintering temperature enhances the reaction layers thickness in the Al-Fe<sub>66</sub>Cr<sub>10</sub>Nb<sub>5</sub>B<sub>19</sub> composite, obtained by the SPS method, leading to its brittleness. Similar dependence can be observed in the samples obtained in the current study. Achieved results demonstrate the higher wear resistance of Al-SHS7574 coatings compared to Al-B<sub>4</sub>C coatings (under the same test conditions) obtained in [29]. Shikalov et al. [29] showed that the boron carbide content in the coatings was significantly lower than in the Al-B<sub>4</sub>C feedstock powder mixture. This indicates a low deposition efficiency of B<sub>4</sub>C. The maximum microhardness value of 84.9 ± 5.8 HV<sub>0.3</sub> was determined for coating with 27 vol% of boron carbide.

Fig. 10 shows 3D images of wear tracks of Al-SHS7574 coatings. It should be noted that the volume loss was calculated as the sum of the volume of squeezed out material and the volume of the worn material.

The polished surface of the coatings was considered as zero level. Fig. 11 shows the cross-sectional 2D profiles of worn surfaces of the Al-SHS7574 coatings. It can be seen that the volume of squeezed out material decreases with increasing annealing temperature of Al-SHS7574 coatings. It is attributed to a decrease in amount of pure aluminum due to its consumption for reaction with the elements of SHS7574 alloy.

The results of SEM investigation of the worn surfaces of the obtained Al-SHS7574 coatings are shown in Fig. 12. Due to the presence of an aluminum matrix the surface morphology of the as-sprayed and heat-treated at 540 °C coatings was characterized by extensive plastic deformation and obvious evidence of smearing (Fig. 12a–b). SHS7574 particles surrounded by reaction layers in the aluminum matrix alloy provide protection to the softer matrix during dry sliding and strengthen it, thus limiting the deformation (Fig. 12b). The high porosity and content of brittle intermetallics in the Al-SHS7574 coating after annealing at 600 °C had a negative effect on wear resistance (Fig. 12c). The worn surface of the coating shows areas where the reaction layers have been flaked off (dark gray areas). Hard delaminated particles of the reaction layers increased the wear rate of the Al-SHS7574 heat-treated composite coatings at 600 °C.

#### 4. Conclusions

The possibility of producing dense coatings by cold spraying a powder mixture of aluminum and partially amorphous Fe-based alloy particles has been shown for the first time. The constitution of the as-sprayed Al-SHS7574 composite coating was nearly the same as that of the initial powder mixture. Post annealing of the coatings at 540 °C and 600 °C promoted the formation of reaction layers consisting of intermetallics, borides and carbides. The hardness and wear resistance of the coatings depended on the annealing temperature. The coating after annealing at 600 °C showed the highest hardness and lowest wear resistance due to the formation of thick brittle reaction layers. Preservation of the aluminum matrix and the formation of thin reaction layers around the Fe-based alloy particles have increased the wear resistance of the composite coatings. The present results clearly showed that cold

spraying of Al-SHS7574 powder mixture with subsequent annealing is a promising process to fabricate coating with an attractive complex of properties.

Further work is currently underway to investigate the phase evolution of the Al-SHS7574 composite coating during heat treatment by in-situ synchrotron X-ray diffraction.

### CRediT authorship contribution statement

**Ivanna D. Kuchumova:** Conceptualization, Methodology, Writing – original draft, Project administration, Funding acquisition. **Vladislav S. Shikalov:** Methodology, Writing – review & editing. **Tomila M. Vidyuk:** Investigation. **Arina V. Ukhina:** Investigation. **Tatyana A. Brusentseva:** Investigation. **Ivan A. Bataev:** Methodology, Funding acquisition. All authors have read and agreed to the published version of the manuscript.

### Declaration of Competing Interest

The authors declare that they have no known competing financial interests or personal relationships that could have appeared to influence the work reported in this paper.

### Data Availability

No data was used for the research described in the article.

### Acknowledgements

The research was conducted at the core facility "Structure, mechanical and physical properties of materials". The study was conducted at the Equipment Sharing Center "Mechanics" of ITAM SB RAS. Ivanna D. Kuchumova acknowledges partial support by the State Contract of Lavrentyev Institute of Hydrodynamics of SB RAS (State Registration Number FWGG-2019-0003) and Ivan A. Bataev acknowledges partial support by the Federal Task of Ministry of Education and Science of the Russian Federation (project FSUN-2020-0014 (2019-0931): "Investigations of Metastable Structures Formed on Material Surfaces and Interfaces under Extreme External Impacts").

### References

- [1] S. Kumar, M. Kumar, N. Jindal, Overview of cold spray coatings applications and comparisons: a critical review, *World J. Eng.* 17 (1) (2020) 27–51, <https://doi.org/10.1108/WJE-01-2019-0021>.
- [2] R.N. Raoelison, Y. Xie, T. Sapanathan, M.P. Planche, R. Kromer, S. Costil, C. Langlade, Cold gas dynamic spray technology: a comprehensive review of processing conditions for various technological developments till to date, *Addit. Manuf.* 19 (2018) 134–159, <https://doi.org/10.1016/j.addma.2017.07.001>.
- [3] S. Yin, P. Cavaliere, B. Aldwell, R. Jenkins, H. Liao, W. Li, R. Lupoi, Cold spray additive manufacturing and repair: fundamentals and applications, *Addit. Manuf.* 21 (2018) 628–650, <https://doi.org/10.1016/j.addma.2018.04.017>.
- [4] Q. Wang, P. Han, S. Yin, W.-J. Niu, L. Zhai, X. Li, X. Mao, Y. Han, Current research status on cold sprayed amorphous alloy coatings: a review, *Coatings* 11 (2) (2021) 206, <https://doi.org/10.3390/coatings11020206>.
- [5] A. Papyrin, V. Kosarev, S. Klinkov, A. Alkimonov, V. Fomin, Cold spray technology. Cold Spray Technology, Elsevier Ltd, 2007, <https://doi.org/10.1016/B978-0-08-045155-8.X5000-5>.
- [6] M. Tului, C. Bartuli, A. Bezzon, A.L. Marino, F. Marra, S. Matera, G. Pulci, Amorphous steel coatings deposited by cold-gas spraying, *Metals* 9 (2019) 678, <https://doi.org/10.3390/met9060678>.
- [7] R. Nikbakht, H. Assadi, K. Jahani, M. Saadati, B. Jodoin, Cold spray deformation and deposition of blended feedstock powders not necessarily obey the rule of mixture, *Surf. Coat. Technol.* 424 (2021), 127644, <https://doi.org/10.1016/j.surfcoat.2021.127644>.
- [8] V.S. Shikalov, T.M. Vidyuk, A.A. Filippov, I.D. Kuchumova, Microstructure, mechanical and tribological properties of cold sprayed CuW coatings, *Int. J. Refract. Met. Hard Mater.* 106 (2022), 105866, <https://doi.org/10.1016/j.ijrmhm.2022.105866>.
- [9] J.S. Kim, Y.S. Kwon, O.I. Lomovsky, D.V. Dudina, V.F. Kosarev, S.V. Klinkov, D. H. Kwon, I. Smurov, Cold spraying of in situ produced TiB<sub>2</sub>-Cu nanocomposite powders, *Compos. Sci. Technol.* 67 (11–12) (2007) 2292–2296, <https://doi.org/10.1016/j.compscitech.2007.01.019>.
- [10] A. Aldhameer, M.S. El-Eskandarany, M. Kishk, F. Alajmi, M. Banyan, Mechanical alloying integrated with cold spray coating for fabrication Cu<sub>50</sub>(Ti<sub>50-x</sub>Ni<sub>x</sub>), x; 10, 20, 30, and 40 at% antibiofilm metallic glass coated/SUS304 sheets, *Nanomaterials* 12 (2022) 1681, <https://doi.org/10.3390/nano12101681>.
- [11] C. Feng, V. Guiport, M. Jeandin, O. Amsellem, F. Pauchet, R. Saenger, S. Bucher, C. Iacob, B<sub>4</sub>C/Ni composite coatings prepared by cold spray of blended or CVD-coated powders, *J. Therm. Spray. Tech.* 21 (2012) 561–570, <https://doi.org/10.1007/s11666-012-9774-x>.
- [12] M. Winnicki, M. Jasiorski, A. Baszczuk, M. Korzeniowski, Heat-treatment of Aluminium-Nickel composite cold sprayed coating, *Coatings* 10 (2020) 581, <https://doi.org/10.3390/coatings10060581>.
- [13] H.T. Wang, C.J. Li, G.J. Yang, C.X. Li, Q. Zhang, W.Y. Li, Microstructural characterization of cold-sprayed nanostructured FeAl intermetallic compound coating and its ball-milled feedstock powders, *J. Therm. Spray. Technol.* 16 (2007) 669–676, <https://doi.org/10.1007/s11666-007-9089-5>.
- [14] T. Novoselova, S. Celotto, R. Morgan, P. Fox, W. O'Neill, Formation of TiAl intermetallics by heat treatment of cold-sprayed precursor deposits, *J. Alloy. Compd.* 436 (2007) 69–77, <https://doi.org/10.1016/j.jallcom.2006.06.101>.
- [15] Z.B. Zhao, B.A. Gillispie, J.R. Smith, Coating deposition by the kinetic spray process, *Surf. Coat. Technol.* 200 (2006) 4746–4754, <https://doi.org/10.1016/j.surfcoat.2005.04.033>.
- [16] H.T. Wang, C.J. Li, G.C. Ji, G. -J. Yang, Annealing effect on the intermetallic compound formation of cold sprayed Fe/Al composite coating, *J. Therm. Spray. Tech.* 21 (2012) 571–577, <https://doi.org/10.1007/s11666-011-9722-1>.
- [17] K. Georgarakis, D.V. Dudina, V.I. Kvashnin, Metallic glass-reinforced metal matrix composites: design, interfaces and properties, *Materials* 15 (23) (2022) 8278, <https://doi.org/10.3390/ma15238278>.
- [18] D.V. Dudina, B.B. Bokhonorov, I.S. Batraev, Y.N. Amirastanov, A.V. Ukhina, I. D. Kuchumova, M.A. Legan, A.N. Novoselov, K.B. Gerasimov, I.A. Bataev, K. Georgarakis, Y. G.Yu. Koga, W.J. Guo, A.M. Botta, Jorge, Interaction between Fe<sub>66</sub>Cr<sub>10</sub>Nb<sub>5</sub>B<sub>19</sub> metallic glass and aluminum during spark plasma sintering, *Mater. Sci. Eng. A* 799 (2021), 140165, <https://doi.org/10.1016/j.msea.2020.140165>.
- [19] W.B. Choi, L. Li, V. Luzin, R. Neiser, T. Gnäupel-Herold, H.J. Prask, S. Sampath, A. Gouldstone, Integrated characterization of cold sprayed aluminum coatings, *Acta Mater.* 55 (3) (2007) 857–866, <https://doi.org/10.1016/j.actamat.2006.09.006>.
- [20] T. Clyne, P. Withers, Applications. In An Introduction to Metal Matrix Composites (Cambridge Solid State Science Series), Cambridge University Press, Cambridge, 1993, pp. 454–473, <https://doi.org/10.1017/CBO9780511623080.013>.
- [21] M.J. Kozcaz, S.C. Khatri, J.E. Allison, M.G. Bader, 1993. Chapter 16 - Metal-Matrix Composites for Ground Vehicle, Aerospace, and Industrial Applications, Fundamentals of Metal-Matrix Composites, Butterworth-Heinemann, (1993) 297–326, <https://doi.org/10.1016/B978-0-08-052371-2.50020-1>.
- [22] W.W. Zhang, Y. Hu, Z. Wang, C. Yang, G.Q. Zhang, K.G. Prashanth, C. Suryanarayana, A novel high-strength Al-based nanocomposite reinforced with Ti-based metallic glass nanoparticles produced by powder metallurgy, *Mater. Sci. Eng. A* 734 (2018) 34–41, <https://doi.org/10.1016/j.msea.2018.07.082>.
- [23] X. Zhu, Z. Yao, X. Gu, W. Cong, P. Zhang, Microstructure and corrosion resistance of Fe-Al intermetallic coating on 45 steel synthesized by double glow plasma surface alloying technology, *Trans. Nonferrous Met.* 19 (1) (2009) 143–148, [https://doi.org/10.1016/S1003-6326\(08\)60242-3](https://doi.org/10.1016/S1003-6326(08)60242-3).
- [24] Ö. Balci, K.G. Prashanth, S. Scudino, M. Somer, J. Eckert, Powder metallurgy of Al-based composites reinforced with Fe-based glassy particles: effect of microstructural modification, *Part. Sci. Technol.* 37 (3) (2019) 286–291, <https://doi.org/10.1080/02726351.2017.1355859>.
- [25] Z. Wang, S. Scudino, M. Stoica, W. Zhang, J. Eckert, Al-based matrix composites reinforced with short Fe-based metallic glassy fiber, *J. Alloy. Compd.* 651 (2015) 170–175, <https://doi.org/10.1016/j.jallcom.2015.08.098>.
- [26] S.V. Klinkov, V.F. Kosarev, V.S. Shikalov, Influence of nozzle velocity and powder feed rate on the coating mass and deposition efficiency in cold spraying, *Surf. Coat. Technol.* 367 (2019) 231–243, <https://doi.org/10.1016/j.surfcoat.2019.04.004>.
- [27] W.C. Oliver, G.M. Pharr, An improved technique for determining hardness and elastic modulus using load and displacement sensing indentation experiments, *J. Mater. Res.* 7 (1992) 1564–1583, <https://doi.org/10.1557/JMR.1992.1564>.
- [28] T. Novoselova, P. Fox, R. Morgan, W. O'Neill, Experimental study of titanium/aluminum deposit produced by cold gas dynamic spray, *Surf. Coat. Technol.* 200 (8) (2006) 2775–2783, <https://doi.org/10.1016/j.surfcoat.2004.10.133>.
- [29] V.S. Shikalov, V.F. Kosarev, T.M. Vidyuk, S.V. Klinkov, I.S. Batraev, Mechanical and tribological properties of cold sprayed composite Al-B<sub>4</sub>C coatings, *AIP Conf. Proc.* 2448 (1) (2021), 020021, <https://doi.org/10.1063/5.0073401>.
- [30] V.F. Kosarev, V.S. Shikalov, M.G. Fouad, T.M. Vidyuk, S.V. Klinkov, Structure and properties of composite coatings cold sprayed from powder mixtures of aluminum and boron carbide, *Sib. J. Phys.* 17 (3) (2002) 47–52, <https://doi.org/10.25205/2541-9447-2022-17-3-47-52>.
- [31] M.M.P. Janssen, G.D. Rieck, Reaction diffusion and kirkendall-effect in the nickel-aluminum system, *Trans. Metall. Soc. AIME* 239 (9) (1967) 1372–1385.
- [32] D.V. Dudina, V.I. Kvanin, A.A. Matvienko, A.A. Sidelnikov, A.I. Gavrilov, A. V. Ukhina, A.M. Jorge Jr., K. Georgarakis, Towards a better understanding of the interaction of Fe<sub>66</sub>Cr<sub>10</sub>Nb<sub>5</sub>B<sub>19</sub> metallic glass with aluminum: growth of intermetallics and formation of kirkendall porosity during sintering, *Chemistry* 5 (1) (2023) 138–150, <https://doi.org/10.3390/chemistry5010011>.
- [33] F. Huang, J. Kang, W. Yue, X. Liu, L. Zh. Fu, D. Zhu, G. She, H. Ma, J. Wang, W. Liang, C. Weng, Wang, Effect of heat treatment on erosion-corrosion of Fe-based amorphous alloy coating under slurry impingement, *J. Alloy. Compd.* 820 (2020), 153132, <https://doi.org/10.1016/j.jallcom.2019.153132>.

- [34] L. Cho, L. Golem, E.J. Seo, D. Bhattacharya, J.G. Speer, K.O. Findley, Microstructural characteristics and mechanical properties of the Al-Si coating on press hardened 22MnB5 steel, *J. Alloy. Compd.* 846 (2020), 156349, <https://doi.org/10.1016/j.jallcom.2020.156349>.
- [35] I.D. Kuchumova, I.S. Batraev, A.V. Ukhina, T.A. Borisenko, U.E. Bulanova, V. Y. Ulianitsky, D.V. Dudina, V.S. Shikalov, V.F. Kosarev, I.A. Bataev, G.Y. Koga, A. M. Jorge Jr., Processing of Fe-based alloys by detonation spraying and spark plasma sintering, *J. Therm. Spray. Tech.* 30 (2021) 1692–1702, <https://doi.org/10.1007/s11666-021-01237-4>.
- [36] I.D. Kuchumova, I.S. Batraev, V.S. N.Yu. Cherkasova, A.V. Shikalov, G.Y. Ukhina, A.M. Koga, Jorge Jr, Wear-resistant Fe-based metallic glass-Al<sub>2</sub>O<sub>3</sub> composite coatings produced by detonation spraying, *J. Therm. Spray. Tech.* 33 (2022) 1355–1365, <https://doi.org/10.1007/s11666-021-01299-4>.
- [37] D.V. Dudina, B.B. Bokhonov, I.S. Batraev, V.I. Kvashnin, M.A. Legan, A. N. Novoselov, A.G. Anisimov, M.A. Esikov, A.V. Ukhina, A.A. Matvienko, K. Georgarakis, G.Y. Koga, A.M. Jorge Jr., Microstructure and mechanical properties of composites obtained by spark plasma sintering of Al-Fe<sub>66</sub>Cr<sub>10</sub>Nb<sub>5</sub>B<sub>19</sub> metallic glass powder mixtures, *Metals* 11 (9) (2021) 1457, <https://doi.org/10.3390/met11091457>.